Walls inhibit chaotic mixing

Emmanuelle Gouillart, N. Kuncio, Olivier Dauchot, Bérengère Dubrulle,

Stéphane Roux, Jean-Luc Thiffeault

▶ To cite this version:

HAL Id: hal-00193177

https://hal.archives-ouvertes.fr/hal-00193177

Submitted on 16 Dec 2007

Walls inhibit chaotic mixing

E. Gouillart,[1] N. Kuncio,[1] O. Dauchot,[1] B. Dubrulle,[1] S. Roux,[2] and J.-L. Thiffeault[3]

[1]*Service de Physique de l'Etat Condensé, DSM, CEA Saclay, URA2464, 91191 Gif-sur-Yvette Cedex, France*
[2]*Surface du Verre et Interfaces, UMR CNRS/Saint-Gobain, 93303 Aubervilliers, France*
[3]*Department of Mathematics, Imperial College London, SW7 2AZ, United Kingdom*
(Dated: April 5, 2007)

We report on experiments of chaotic mixing in a closed vessel, in which a highly viscous fluid is stirred by a moving rod. We analyze quantitatively how the concentration field of a low-diffusivity dye relaxes towards homogeneity, and observe a slow algebraic decay of the inhomogeneity, at odds with the exponential decay predicted by most previous studies. Visual observations reveal the dominant role of the vessel boundary, which strongly influences the concentration field in the entire domain and causes the anomalous scaling. A simplified 1-D model supports our experimental results. Quantitative analysis of the concentration pattern leads to scalings for the distributions and the variance of the concentration field consistent with experimental and numerical results.

Low-Reynolds-number fluid mixing has a variety of applications ranging from geophysics to industrial mixing devices. While turbulent flows lead to highly efficient mixing, simple laminar flows with chaotic Lagrangian dynamics also promote rapid homogenization [1]. Dynamical systems approaches based on flow kinematics have provided a first insight into chaotic mixing [2, 3]. A deeper understanding of homogenization processes is gained by examining the interplay between chaotic stirring and diffusion. Several experimental [4, 5] and numerical [6, 7] studies obtained an exponential decay for the variance of a diffusive scalar concentration field in a chaotic mixer. This behavior is attributed to an asymptotic spatial structure of the scalar dubbed *strange eigenmode* [8], that results in a global exponential decay of the spatial contrast. However, these theories focus on ideal mixing systems, *e.g.* with periodic or slip boundary conditions, far from the reality of industrial mixing devices with solid no-slip walls. It has been suggested [9, 10] that mixing might be slower in bounded flows, but experimental evidence is still lacking.

In this Letter, we study experimentally dye homogenization by chaotic mixing in a 2-D closed flow. Precise measurements of the concentration field yield "slow" algebraic decay of an inhomogeneity, at odds with the expected exponential decay. We relate quantitatively this slow mixing to the chaotic nature of trajectories initially close to the no-slip wall, which end up escaping in the bulk and slow down the whole mixing process.

A cylindrical rod periodically driven on a figure-eight path gently stirs viscous sugar syrup inside a closed vessel (Fig. 1 (a)). The stirring scale is comparable to the vessel size, in contrast to other devices such as arrays of magnets [4, 5]. This protocol is a good candidate for efficient mixing: we can observe on a Poincaré section (Fig. 1 (a)) – computed numerically for the corresponding Stokes flow – a large chaotic region spanning the *entire* domain, including the vicinity of the wall. The signature of chaotic advection can also be observed in Fig. 1 (a), where a complex lamellar pattern

is created by the stretching and folding of an initial dye blob into exponentially thin filaments. The fluid viscosity $\nu = 5 \times 10^{-4}\,\mathrm{m}^2 \cdot \mathrm{s}^{-1}$ together with rod diameter $\ell = 16\,\mathrm{mm}$ and stirring velocity $U = 2\,\mathrm{cm} \cdot \mathrm{s}^{-1}$ yield a Reynolds number $Re = U\ell/\nu \simeq 0.6$, consistent with a Stokes flow regime. A spot of low-diffusivity dye (Indian ink diluted in sugar syrup) is injected at the surface of the fluid, and we follow the evolution of the dye concentration field during the mixing process (see Fig. 1). The concentration field is measured through the transparent bottom of the vessel using a 12-bit CCD camera at resolution 2000×2000.

Despite the exponential stretching occurring in the bulk, the resulting variance $\sigma^2(C)$ of the concentration field (measured in a large central rectangular region) decays surprisingly slowly with time t as a power law t^{-m} with $m \simeq 3.2$ (Fig. 1 (b)), and not exponentially as expected. This behavior persists until the end of the experiment (35 periods), by which time the variance has decayed by more than three orders of magnitude. Moreover, concentration probability distribution functions (PDFs) shown on Fig. 1 (c) exhibit wide power-law tails on both sides of the most probable value. The probability of "white" (zero) concentration decays very slowly with time, whereas the peak shifts towards lower values.

In order to understand these surprising scalings, we first describe the various mechanisms at play during the mixing process. A blob of dye, initially released close to the vessel center, is transformed into a complicated pattern expanding towards the boundary with time. We distinguish at each instant the growing "mixed region", delimited by the advected blob frontier, and the remaining boundary region where $C = 0$, in the vicinity of the vessel wall. This distinction is obvious in Fig. 1 (a) where one can observe a central heart-shaped mixed region and an annular unmixed boundary region. As the chaotic region spans the entire flow, fluid particles initially close to the zero-velocity wall eventually escape from the boundary to wander through the whole chaotic region. Trajectories escape along the unstable manifold of parabolic
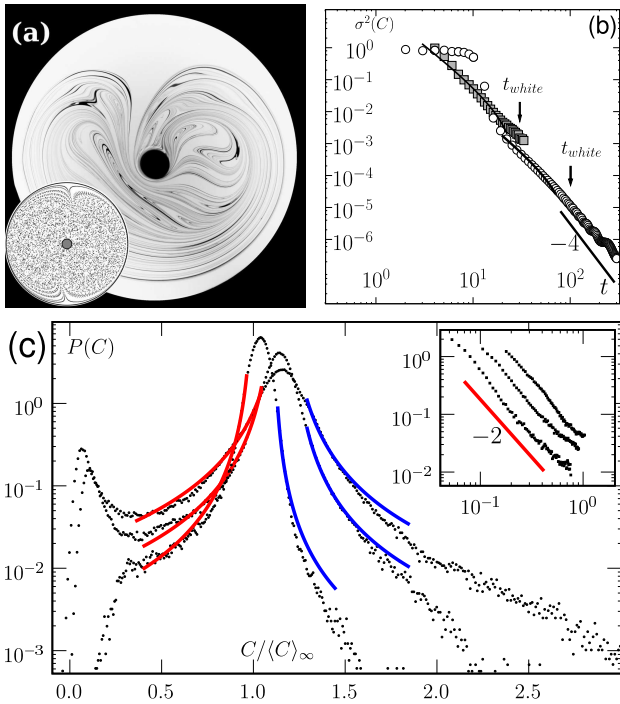
FIG. 1: (a) Chaotic mixing experiment in a closed vessel: a rod moves periodically on a figure-eight path (see Fig. 2 (a)) and transforms an initial spot of dye into a complicated filamentary pattern. Inset: Poincaré section obtained numerically for the corresponding Stokes flow. Note that the chaotic region spans the entire domain. (b) Evolution of the variance of the concentration field in a fixed central region. ■: experiment , ○: numerical simulation (see Fig. 3 for a description). Solid line fits: contribution of the white pixels $\sigma_W^2 \simeq (2\log t + \log w_B)/(\log\Gamma \times t^2)$ derived below. (c) Experimental concentration PDFs in the bulk at time $t = 13, 17, 31$ periods. Both sides of the peak can be fitted by power laws $(C_{max} - C)^{-2}$ (red and blue plots). Inset: left ("light-gray") tail of the peak, $P(C)$ against $|C_{max}(t) - C|$.

separation points on the boundary [3, 11]. The signature of such an escape path can be visualized on Fig. 1 (a) where unmixed fluid from the boundary is "sucked" inside the mixed region through its white cusp, close to the rod. This results in the periodic injection of broad white strips that can be observed inside the mixed region. The mixing region then grows towards the boundary to make up for this mass injection. Incompressibility combined with zero-velocity condition at the boundary leads [9] to a shrinking distance between the mixed region border and the boundary scaling as $d(t) \propto t^{-1}$. This scaling is verified experimentally. The area of unmixed fluid from the boundary injected at each period inside the mixed region then scales as $\dot{d}(t) \propto t^{-2}$. As a result, the mean concentration value inside the bulk decreases with time as $(1 - d(t))^{-1}$. Simultaneously, the mixed region is stretched and folded at each half-cycle of the rod movement (see Fig. 2 (a)) in a baker's-map-like fashion [12].

However, it should be noted that the two folded parts are not stacked directly onto each other but *separated by the newest injected white strip*. Also note that the part "attached" to the rod has experienced more stretching than the one "left behind". Briefly, (i) chaotic stretching imposes that the typical width of a dye filament in the bulk shrinks exponentially down to the diffusion or measurement scale, yet (ii) wide strips of unmixed fluid of width $\dot{d}(t) \propto 1/t^2$ are periodically inserted between these fine structures. In the following we derive how these two effects lead to the observed scalings.

For this purpose, we simplify the 2-D problem by characterizing only 1-D concentration profiles $C(x, t)$ along a secant to the stretching direction – the dashed segments on Fig. 2 (a) – that is, we neglect the variation of the concentration along a dye filament on a scale comparable to the vessel size. We thus call from now on "mixed region" the intersection of the 2-D mixed region with such a segment. The effect of the mixer during a half-period then amounts to the action of a one-dimensional discrete-time map that transforms concentration profiles by inserting an interval of width $\dot{d}_t$ of fluid from the boundary between two inhomogeneously compressed images of the mixing region at the previous time (see Fig. 2 (a)). Such a map f, defined on $[0, 1]$ for simplicity, evolves concentration profiles as $C(x, t + 1) = C(f^{-1}(x), t)$ and meets the following requirements: (i) it is a continuous double-valued function to account for the stretching/folding process; (ii) $x = 0$ is a marginally unstable point of f^{-1}; the correct dynamics close to the boundary are indeed reproduced by imposing $f^{-1}(x) \simeq x + ax^2 + \cdots$, $a > 0$ for small x; (iii) because of mass conservation, at each x, the local slopes of the two branches add up to 1. Other details of f are unessential for our discussion. Diffusion is mimicked by letting the concentration profile diffuse between successive iterations of the map. This model is a modified baker's map [12], with a parabolic point at $x = 0$, whereas the dynamics are purely hyperbolic in a classical baker's map. Numerical simulations for a specific choice of f lead to results shown in Fig. 1 (b) and Fig. 3: both the power-law evolution of the variance and the different aforementioned features of the experimental PDFs are reproduced by the simulations.

The map transforms an initial blob of dye of width s_0 into an increasing number of strips with widths $s_0\gamma_1 \cdots \gamma_t$, resulting from different stretching histories inside the mixed region, where γ_t is the compression experienced at time t. White strips also experience this multiplicative stretching from their injection time. As the mixed region grows towards the boundary, different values of stretching will be sampled. It will nevertheless be justified below that the concentration measures only require knowledge of the stretching histories traced back during a finite number of periods. This allows us to define in a "quasi-static" approximation a slowly varying instantaneous "Lyapunov exponent"
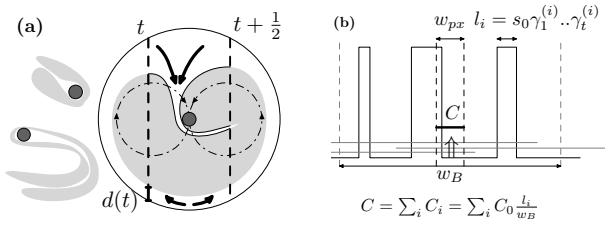
FIG. 2: (a) Transport mechanisms: (i) the rod stretches and folds the mixed region and (ii) a white strip of unmixed fluid is injected between the two folded parts. (b) Stretched strips of dye (black) are smeared out by diffusion on a scale w_B (gray). The concentration C of a pixel x is then given by adding the concentrations coming from strips inside a box of size w_B around x.
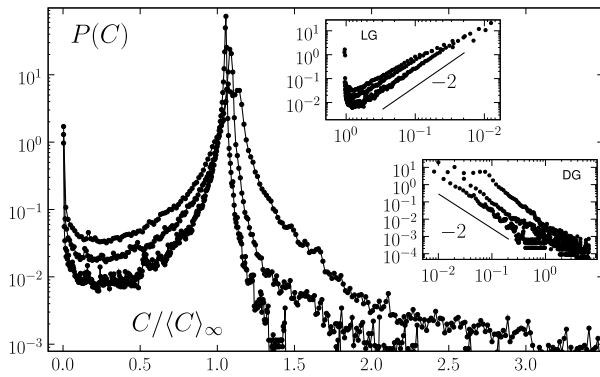

FIG. 3: Numerical concentration PDFs ($t = 15, 18, 25$) obtained by letting concentration profiles evolve as $C(x,t+1) = C(f^{-1}(x),t)$, $f(x) : f_1(x) = x - ax^2 + (\gamma - 1 + a)x^3$; $f_2(x) = 1 - ax^2 + (\gamma - 1 + a)x^3$ with $a = 0.9$ and $\gamma = 0.55$. Upper (resp. lower) inset: light (resp. dark) gray tail, $P(C)$ against $|C_{max} - C|$. We observe the same power-law decay $(C_{max} - C)^{-2}$ on both sides of the maximum as in the experiment (Fig. 1 (c)).

$\Gamma(t) = \exp(\langle -\log(|\frac{\partial f^{-1}(x)}{\partial x}|)\rangle_{MR})$, that is the geometric mean of the compression taken over the mixed region (MR) at time t. Note that as the white strips are injected close to the center of the domain, the two branches of f have comparable mean slopes, yielding the estimate $\Gamma \sim 0.5$. Without diffusion, dye strips would have a typical width $s_0 \Gamma^t$ at time t. However, the balance between stretching and diffusion imposes that the width of a strip stabilizes at the Batchelor scale $w_B = \sqrt{\kappa/(1 - \Gamma^2)}$, where κ is the diffusion coefficient. w_B is thus the smallest lengthscale that can be observed in the concentration profile, and different elementary strips may overlap (Fig. 2 (b)). Since the concentration field is probed by averaging it on the pixel size w_{px}, which is smaller than w_B, the concentration at a pixel is given by adding the contributions from strips contained in a box of size w_B around the pixel. Hence we characterize $P(C)$ by considering the different combinations of strip widths for a

zero-diffusivity dye – the concentration profile on Fig. 2 (b) – that one might find in a box of size w_B. We will distinguish between three generic cases corresponding to three different regions of the histogram $P(C)$ (see Fig. 1 (c) and Fig. 3): a white (W) peak at $C = 0$ corresponding to injected white strips still wider than w_B, light gray (LG) and dark gray (DG) tails corresponding to respectively smaller and larger concentrations than the peak (mean) concentration. Once we have quantified the proportion of boxes contributing to these different values of C, the variance will be readily obtained as

$$\sigma^2(C) = \int (C - \langle C \rangle)^2 P(C) \mathrm{d}C = \sigma_W^2 + \sigma_{LG}^2 + \sigma_{DG}^2. \quad (1)$$

Let us start with white (zero) concentration measures that come from the stretched images of white strips injected before t. White strips injected at an early time have been stretched and wiped out by diffusion, that is their width has become smaller than w_B. Hence the oldest white strips that can be observed have been injected at the time $t_i(t)$ such that $\dot{d}_{t_i} \Gamma^{t-t_i} = w_B$. Note that from t_{white} defined by $\dot{d}_{t_{white}} = w_B$, the injected white strip is smaller than w_B and no white pixels can be observed. Before t_{white}, the number of white pixels is proportional to $n_W = d_{t_i(t)} - d_t \propto (t - t_i)(t_i t)^{-1}$ for large t (using $d_t \propto t^{-1}$). As $t - t_i \simeq (2 \log t + \log w_B)/\log \Gamma$, $n_W \simeq (2 \log t + \log w_B)/(\log \Gamma \times t^2)$. We deduce $\sigma_W^2 \simeq (2 \log t + \log w_B)/(\log \Gamma \times t^2)$ for $t < t_{white}$ and $\sigma_W^2 = 0$ after t_{white}.

We now concentrate on the distribution of light gray values corresponding to white strips that have just been compressed below the cut-off scale w_B. We propose to approximate the measured value C as the average of the biggest white strip with width $\lambda < w_B$, and mixed "gray" fluid whose concentration is close to the most probable concentration C_g. A box with a white strip of scale λ thus bears a concentration $C_\lambda = C_g(1 - \lambda/w_B)$ and we can relate $P(C)$ to the distribution of widths of the images of the injected white strips $Q(\lambda)$. A white strip injected at t_0 is transformed into 2^{t-t_0} images with scales $\dot{d}_{t_0} \Gamma^{t-t_0}$. Therefore $Q(\lambda) = (\lambda/\dot{d}_{t_0})^{\log(2)/\log(\Gamma)} \times (1/\lambda \log \Gamma)$, resulting in

$$P(C) = \dot{d}_t^{\log 2/\log(\Gamma^{-1})} \frac{w_B}{C_g(t)} \left[w_B\left(1 - \frac{C}{C_g}\right) \right]^{\frac{\log 2}{\log \Gamma} - 1}$$

$$= g(t)\left[C_g - C \right]^{(\log 2/\log \Gamma) - 1}. \quad (2)$$

$P(C)$ thus has a power-law tail in the light gray levels whose exponent depends on the mean stretching Γ. We observe satisfactory agreement between this prediction and both experimental data and numerical 1-D simulations (see Fig. 1 (c) and Fig. 3) where for this tail $P(C) \propto (C - C_g)^{-\alpha}$ with $\alpha \lesssim 2$, consistent with $\Gamma \lesssim 0.5$, a rather homogeneous stretching. Also note that the amplitude of the light-gray tail decreases as a power law

$g(t) \propto \dot{d}_t^{\,\log 2/\log(1/\Gamma)} \propto t^{-2(\log 2/\log(1/\Gamma))}$. We deduce

$$\sigma_{LG}^2 = g(t) \int_{C_{min}}^{C_g} (C_g - C)^{2-\alpha(\Gamma)} dC$$

where $\alpha(\Gamma) = 1 - \log 2/\log \Gamma$, and C_{min} is the smallest concentration observed ($C_{min} = 0$ for $t < t_{white}$ and $C_{min} = C_g(1 - \dot{d}_t/w_B)$ for $t > t_{white}$). For $t < t_{white}$ the integral is constant and $\sigma_{LG}^2 \propto g(t) \propto \dot{d}_t \propto t^{-2}$. On the other hand, for $t \geq t_{white}$,

$$\sigma_{LG}^2 = \frac{g(t)}{2 + \alpha(\Gamma)} [C_g - C_{min}]^{3-\alpha(\Gamma)} \propto t^{-(6+2\frac{\log 2}{\log \Gamma})}.$$

For $\alpha(\Gamma) \sim 2$ as we observed, the exponent in the above power law is about -4.

Finally, the dark gray tail corresponds to boxes containing images of mixed regions from early times – thus with an important percentage of black – that have experienced little stretching. It is therefore not sufficient to consider only the mean stretching Γ as before, since stretching histories far from the mean are involved. Using the large-deviation function S for the finite-time Lyapunov exponents distribution [15], we derive

$$P(C,t) = \frac{2^{t-t_0} \exp[-(t-t_0)S(-\frac{\log w_B}{t-t_0} + \log \Gamma)]}{(C - \langle C \rangle)^2 (t - t_0)^2},$$

where $t_0(C)$ is the earlier time at which the mixed region had a mean concentration C, so that $C = \langle C \rangle (1 - d_{t_0})^{-1}$. At a fixed time the dark gray tail decreases as the dominant contribution $(C - \langle C \rangle)^{-2}$, however the probability to observe a fixed concentration value decays exponentially, allowing us to neglect σ_{DG}^2 in (1). Both the $(C - \langle C \rangle)^{-2}$ shape and the rapid fall-off of the dark-gray tail can be observed on Fig. 1 (c) and Fig. 3.

We now sum these contributions to obtain $\sigma^2(C)$. In the experiment, the crossover t_{white} is estimated as 30 periods. However, 3-D effects inside the fluid prevented us from conducting experiments for more than 35 periods. For this early regime, fitting the data with $\sigma_W^2 \propto (2\log t + \log w_B)/t^2$ (black line on Fig. 1 (b)) gives good results, except close to t_{white} where the contribution of the light gray tail starts to dominate. In contrast, in numerical simulations we observe (Fig. 1 (b)) both the $(2\log t + \log w_B)/t^2$ behavior (black line), which can be interpreted as in the experiment, and the t^{-4} decay after t_{white} (100 periods for the case studied) given by σ_{LG}^2.

Note finally that the algebraic nature of $d(t)$ permits crude "first-order" approximations such as considering only the mean stretching given by the Lyapunov exponent as we did. The injection process dominates other mechanisms put forward to analyze concentration distributions, such as the evolution of the distribution by self-convolution due to the random addition of concentration levels [13, 14]. The strange eigenmode formalism also fails to describe this nonasymptotic regime as the spatial mixing pattern is still evolving.

In conclusion, we propose a universal mixing scenario for mixers with fixed walls belonging to a chaotic region. The injection of unmixed fluid from the boundary inside the bulk affects the whole concentration field, no matter how far from the walls. The algebraic scalings for the variance and concentration distributions can be predicted by studying in physical space the filament-like stirring pattern generated by the combination of stretching, folding, and injection of fluid from the boundaries. Our reasoning could be extended to other algebraic expressions of $d(t)$ resulting from different hydrodynamics at the wall. In the present case (no-slip wall), we derive a power-law (asymptotically t^{-4}) evolution for the decay of the concentration variance, and we find very good agreement between our analytical analysis, experimental and numerical results. Let us briefly mention that Stokes flow simulations of the well-studied blinking vortex flow [1, 3] also yield the same algebraic decay for the variance of a coarse-grained concentration, obtained by advecting a large number of points [16]. Future work will address the generalization of our approach to other systems characterized by continuous injection of inhomogeneity, such as open flows.

[1] H. Aref, J. Fluid Mech. **143**, 1 (1984).
[2] C. W. Leong and J. M. Ottino, J. Fluid Mech. **209**, 463 (1989); J. M. Ottino, *The Kinematics of Mixing: Stretching, Chaos, and Transport* (Cambridge University Press, Cambridge, U.K., 1989).
[3] S. C. Jana, G. Metcalfe and J. M. Ottino, J. Fluid Mech. **269**, 199 (1994).
[4] M.-C. Jullien, P. Castiglione and P. Tabeling, Phys. Rev. Lett. **85**, 3636 (2000).
[5] D. Rothstein, E. Henry and J. P. Gollub, Nature (London) **401**, 770 (1999).
[6] D. R. Fereday and P. H. Haynes, Phys. Fluids **16**, 4359 (2004).
[7] D. R. Fereday, P. H. Haynes, A. Wonhas and J. C. Vassilicos, Phys. Rev. E **65**, 035301 (2002).
[8] R. Pierrehumbert, Chaos Solitons Fractals **4**, 1091 (1994).
[9] M. Chertkov and V. Lebedev, Phys. Rev. Lett. **90**, 034501 (2003).
[10] A. A. Schekochihin, P. H. Haynes and S. C. Cowley, Phys. Rev. E **70**, 046304 (2004).
[11] G. Haller, J. Fluid Mech. **512**, 257 (2004).
[12] J. D. Farmer, E. Ott and J. A. Yorke, Physica D **7**, 153 (1983).
[13] E. Villermaux and J. Duplat, Phys. Rev. Lett. **91**, 184501 (2003).
[14] A. Venaille and J. Sommeria, arXiv:physics/0603225.
[15] E. Ott, *Chaos in Dynamical Systems* (Cambridge University Press, Cambridge, U.K., 1994).
[16] Results of these numerical experiments will be presented in a paper in preparation.